J Mater Sci: Mater Electron
DOI 10.1007/s10854-016-6177-7

Effect of complexing agent on the chemically deposited ZnS thin film

Priyanka U. Londhe[1] · Ashwini B. Rohom[1] · Ganesh R. Bhand[1] · Sujata Jadhav[1] · Manorama G. Lakhe[1] · Nandu B. Chaure[1]

Received: 14 October 2016 / Accepted: 1 December 2016

Abstract Zinc sulfide (ZnS) thin films have been deposited onto fluorine doped tin oxide and microscopic glass substrates from an aqueous alkaline reaction by chemical bath deposition. The effect of concentrations of hydrazine hydrate (HyH) (complexing agent) on the deposit is studied. X-ray analysis confirm the growth of nanocrystalline ZnS thin films with reflections (111), (220) and (311) correspond to cubic crystalline phase. TEM results support the growth of cubic ZnS layers. The energy band gap was successfully tailored from 2.77 to 3.80 eV. Photoluminescence study indicates a strong band-edge emission with some defect like vacancies. It was also noticed that HyH plays an important role on the nucleation. The remarkable improvement in the growth rate of ZnS thin films have been observed upon increasing the contents of HyH. Nearly stoichiometric ZnS layer was obtained upon annealing prepared with 2.5 M HyH. The crystallinity was found to be increased upon annealing the layers. The ideality factor for the ZnS layers prepared with 0 and 1.0 M HyH were obtained ~1.71 and 1.24, respectively. The capacitance–voltage plots behave according to Schottky–Mott theory. The doping concentrations ~10^{17} and 10^{18} cm^{-3} were calculated for the layers deposited with 0 and 1.0 M HyH, respectively.

✉ Nandu B. Chaure
n.chaure@physics.unipune.ac.in

[1] Electrochemical Laboratory, Department of Physics, Savitribai Phule Pune University (Formerly University of Pune), Pune 411007, India

1 Introduction

Zinc sulfide (ZnS) is a promising material for device applications due to its high refractive index and high transmittance in the visible region. It is extensively used for the development of light emitting diode for blue to ultraviolet spectral region due to its wide band gap, 3.70 eV which can be tailored [1, 2]. It is an excellent host material for the electroluminescent phosphors, which is being commercially used in displays [3]. It is also widely used as buffer layer for solar cell applications. Conventionally, CIGS thin film solar cells are fabricated using CdS buffer layer to form heterojunction and adjust appropriate interface charges [4]. CIGS based thin film solar cells are developed with chemically deposited CdS buffer layer and measured the best efficiencies ~21.7% [3]. It is well known that CdS buffer layer plays an important role in the development of thin film solar cells, however; it may causes serious environmental problems due to the large amount of Cd-containing waste resulting from the deposition process [6, 7]. ZnS may be one of the alternatives to produce Cd-free solar cell devices [4]. Cd-free buffer materials such as ZnS, $Zn(OH)_2$, ZnO, ZnSe, In_2S_3, and InSe have been investigated as an alternative to CdS buffer layer [8–13]. Several methods such as, chemical vapor deposition [14], pulsed-laser deposition [15], RF reactive magnetron sputtering [16], atomic layer deposition [18], spray pyrolysis [19], sol–gel [20], and electrodeposition [21] have been employed to produce ZnS thin films. Among the non-vacuum processes, CBD has been widely used due to its simplicity, cost-effectiveness and suitable for large-area growth. In this process the deposition conditions such as, pH, bath temperature, agitation, growth duration, etc. are important to tune the optical, electrical and morphological properties of the precursor layer. Several researchers have studied the effect of annealing and

various other parameters on the structure and luminescence properties of ZnS thin films. However, the impact of complexing agent on the properties of ZnS thin film has not been addressed thoroughly. Herein, we have reported the effect of complexing agent on the properties of the deposit.

2 Experimental

2.1 Materials details

Zinc Sulphate ($ZnSO_4$), thiourea (H_2NCSNH_2), and hydrazine hydrate (N_2H_4) of purity at least 99.99% were purchased from Alfa Aesar (Germany). Ammonium hydroxide (NH_4OH) was purchased from Thomas Baker of purity 99.9% to adjust the pH of electrolyte. All chemicals were of analytical reagent grade (AR) and used as received. FTO coated glass substrates with sheet resistance ~10 Ω/cm^2 were purchased from Pilkington, UK. Double distilled deionized water was used as a solvent.

2.2 Material synthesis

ZnS thin films have been deposited on FTO coated glass substrates and microscopic glass slides by chemical bath deposition (CBD) technique from aqueous bath consisting 50 mM $ZnSO_4$, 60 mM H_2NCSNH_2 and various concentrations of N_2H_4 viz, 0, 0.5, 1, 1.5 and 2.5 M. The pH of the final growth solution was adjusted to 9 with NH_4OH. The substrates were placed vertically inside the container. The temperature of the solution was maintained ~85 °C during the growth of a layer. Immediately after the deposition, the samples were ultrasonicated in the warm double distilled de-ionized water to remove the traces of loosely bonded particles. The samples were annealed at 450 °C for 2 h in air an ambient. The effect of the concentrations of hydrazine hydrate (HyH) and heat treatment on the deposit were studied by X-ray diffractometry (XRD), UV–vis-NIR absorption spectroscopy, photoluminescence spectroscopy, scanning electron microscopy (SEM), transmission electron microscopy (TEM), energy dispersive X-ray analysis (EDAX), current–voltage (I–V) and capacitance–voltage (C–V) measurement.

2.3 Characterizations

The structural, morphological, compositional and optical properties of as-prepared and heat treated layers were studied using X-ray diffractometer model Bruker D8 advance with Cu Kα radiation of wavelength $\lambda = 1.5405$ Å, JEOL JSM-6360A SEM at accelerating voltage 20 kV and probe current 1 nA, transmission electron microscopy (TEM) model, TECNAI G2, JASCO UV-vis-NIR spectrophotometer and Perkin Elmer LS 55 Photoluminescence (PL) spectrometer. Emission spectra of the samples were recorded at exciton wavelength 325 nm. The Potentiostat, SP 150, Biologic consists two probe measurement setup was employed to study the electrical (*I–V* and *C–V*) properties.

3 Results and discussion

3.1 Reaction mechanism

The deposition of ZnS thin film proceeds when the ionic product of Zn^{2+} and S^{2-} exceeds the solubility product, (Ksp). Since the solubility product of ZnS is very small (10–24.7) [22], the precipitation is expected even at low S^{2-} concentrations, which results the deposition of ZnS difficult. Therefore, the CBD process depends on the slow discharge of precursor ions in the solution. $ZnSO_4$ and thiourea hydrolyzed in an alkaline medium as per to the following reactions,

$$ZnSO_4 \rightarrow Zn^{2+} + SO_4^{2-} \quad (1)$$

$$CS\left(NH_2\right)_2 + 2OH^- \rightarrow S^{2-} + CH_2N_2 + 2H_2O \quad (2)$$

The complexing agent plays an important role on the various properties especially the adhesion and morphology can be altered. Here, HyH has been used as complexing agent which is expected to forms the complex with Zn^{2+} ions by following reaction,

$$Zn^{2+} + 3N_2H_4 \rightarrow \left[Zn\left(N_2H_4\right)_3\right]^{2+} \quad (3)$$

The zinc tetramine $[Zn(N_2H_4)_3]^{2+}$ complex normally undergo heterogeneous reaction with sulfide ions on the substrate by the following reaction;

$$\left[Zn\left(N_2H_4\right)_3\right]^{2+} + S^{2-} \rightarrow ZnS + 3\left(N_2H_4\right) \quad (4)$$

3.2 Structural analysis

Figure 1 shows XRD patterns of the as-deposited ZnS layers deposited with different concentrations of HyH. The diffraction peaks attributed at 2θ = 28.51°, 47.51° and 56.31° correspond to (111), (220) and (311) plane of cubic zinc blende structure, respectively (JCPDS card No.77-100). XRD spectra for the layers deposited without HyH exhibited the reflections associated to $Zn(OH)_2$, which was disappeared upon annealing and the peaks related to ZnS could be seen in the inset figure. The crystallinity of the sample was estimated by measuring the FWHM. The

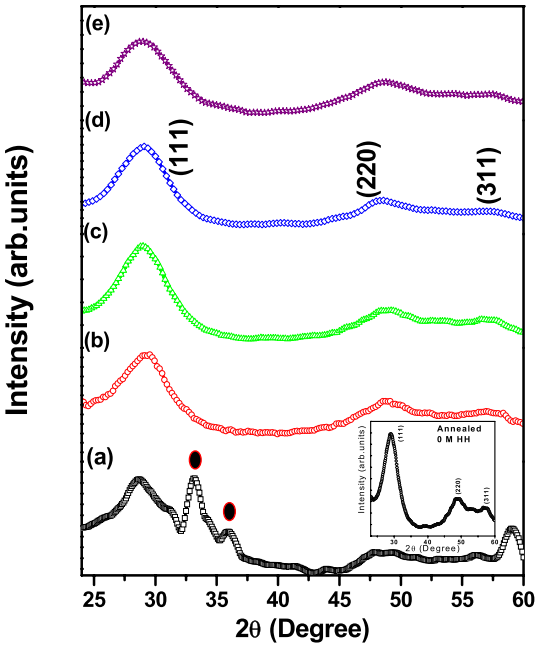

Fig. 1 XRD patterns of as-deposited ZnS thin films prepared for ***a*** 0 M, ***b*** 0.5 M, ***c*** 1.0 M, ***d*** 1.5 M, ***e*** 2.5 M HyH concentration. *Inset* shows the XRD pattern of the annealed ZnS thin film deposited in presence of 0 M HyH. The reflections correspond to $Zn(OH)_2$ are marked by *solid circles* (●)

FWHM was found to be increased systematically upon increasing the contents of HyH in the bath, which could be associated to the particle size. The change in FWHM was further correlated with the average crystallite size calculated by Scherrer formula. The calculated values of FWHM and average particle size are tabulated in Table 1. The values of average crystallite size are in agreement with the increased values of FWHM. Figure 2 shows the HRTEM of the ZnS thin film deposited in presence of 2.5 M HyH. The interplanner distance 'd' obtained by HRTEM analysis was 3.00 Å, which corresponds to (111) reflection of the cubic structure of ZnS. Furthermore, the particle size ~5 to 7 nm can be clearly seen from HRTEM image. The selected area diffraction (SAD) pattern (shown inset) exhibits ring due to the random orientation of the crystallites correspond to (111), (204)/(220) and (311) planes of cubic ZnS. These results are in good agreement with the structural data obtained by XRD analysis.

3.3 Morphological analysis

Figure 3 shows the SEM images of as-deposited and annealed ZnS thin layer deposited for different concentrations of HyH. Granular, spherical particles are deposited

Table 1 FWHM and crystallite size calculated for ZnS reflections from XRD data results

ZnS samples (concentration of HyH in M)	Observed peaks with FWHM (deg)			Average crystallite size estimated from Scherrer's formula (nm)
	(111)	(220)	(311)	
0	2.90	2.27	2.90	32
0.5	3.29	2.49	3.13	29
1.0	3.42	3.01	3.52	25
1.5	3.90	3.24	3.75	23
2.5	4.37	3.87	3.94	21

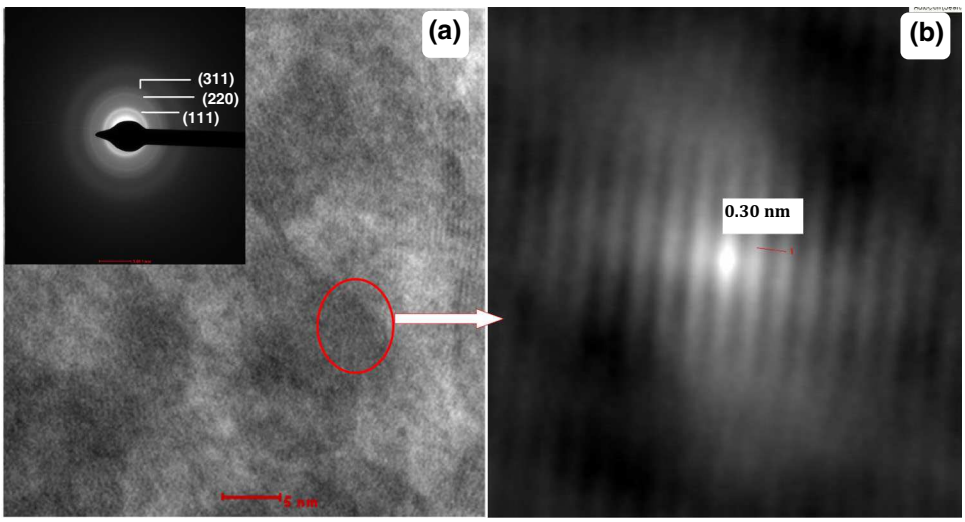

Fig. 2 HRTEM of the ZnS thin film deposited in presence of 2.5 M HyH concentration

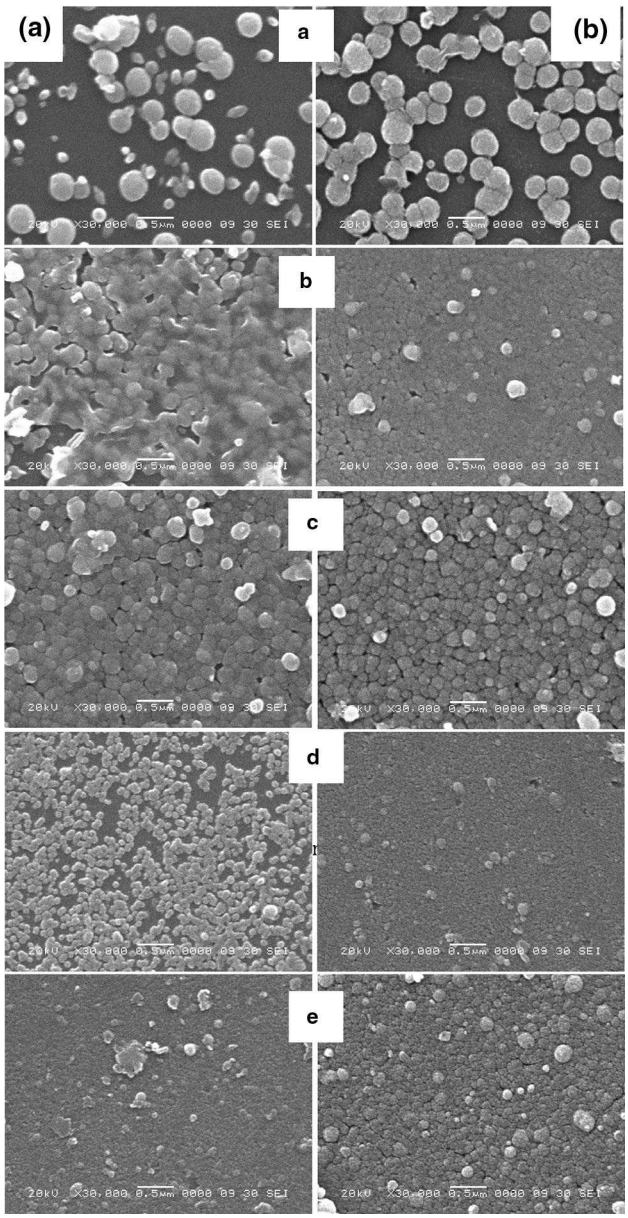

Fig. 3 SEM images of as-deposited (**A**) and annealed (**B**) ZnS thin films prepared at ***a*** 0 M, ***b*** 0.5 M, ***c*** 1.0 M, ***d*** 1.5 M, ***e*** 2.5 M HyH concentration

for all concentrations of HyH. Large spherical individual particles are deposited without HyH can be clearly seen in Fig. 3a. Uniform, compact and well adherent films were deposited in presence of HyH. A uniform growth is associated to the rate of reaction and nucleation centers. The formations of nucleis at the beginning of the deposition process could be responsible for uniform growth of layer. The conductivity of electrolyte is expected to be low for lower concentration of HyH, therefore the reaction rate may be less, which results limited nucleation centers. However, upon increasing the deposition time, the nucleated particles are expected to grow further to form the large clusters. On the contrary, the reactions rate is proposed to be increased for higher concentration of HyH support the growth of smaller particles. Upon annealing the layers at 450 °C for 2 h the densely packed grain growth with an enhancement in the size of the particle. The Elemental composition of the films was obtained by EDAX analysis is tabulated in Table 2. It was observed that the concentration of HyH controlled the contents of precursor layer. The atomic percentage concentration of Zn reduced systematically upon increasing the concentration of HyH in the growth solution and nearly stoichiometric ZnS layer was deposited in presence of 2.5 M HyH.

3.4 Optical study

The absorption coefficient (α) was determined using the expression,

$$\alpha h\nu = k\left(h\nu - E_g\right)^{\frac{n}{2}} \tag{5}$$

where, 'k' is constant, 'E_g' is the energy band gap estimated from UV–Visible results, and n is a constant which is taken to be 1 for direct band gap semiconductors. Figures 4 and 5 shows a plot of $(\alpha h\nu)^2$ versus $h\nu$ of as-deposited and annealed samples, respectively. The band gap values are estimated from the intercept of the straight-line portion of the curve. The estimated energy band gaps are summarized in Table 3. It has been observed that upon increasing the concentration of HyH the band gap of ZnS layer was found to be increased, due to the deposition of

Table 2 A summary of the atomic percentage composition of Zn and S determined in ZnS thin films deposited for various molar concentrations of HyH

HyH concentration	Atomic (%) percentage of elemental Zn and S in ZnS films					
	As-deposited			Annealed		
	Zn	S	Zn/S	Zn	S	Zn/S
0 M	58.04	41.96	1.38	47.16	52.84	0.89
0.5 M	56.35	43.65	1.29	55.82	44.18	1.26
1.0 M	54.94	45.26	1.21	54.31	45.69	1.19
1.5 M	47.62	52.38	0.91	54.41	45.59	1.20
2.5 M	44.82	55.18	0.81	49.87	50.13	1.00

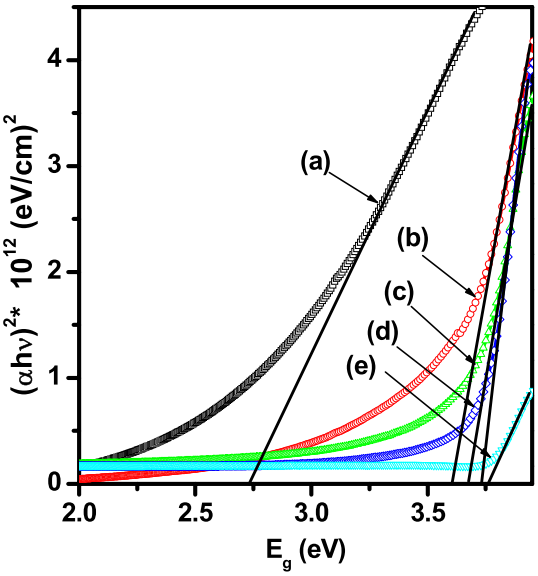

Fig. 4 Plot of $(\alpha h\nu)^2$ versus $(h\nu)$ for as-deposited ZnS thin films prepared with ***a*** 0 M, ***b*** 0.5 M, ***c*** 1.0 M, ***d*** 1.5 M, ***e*** 2.5 M HyH concentrations

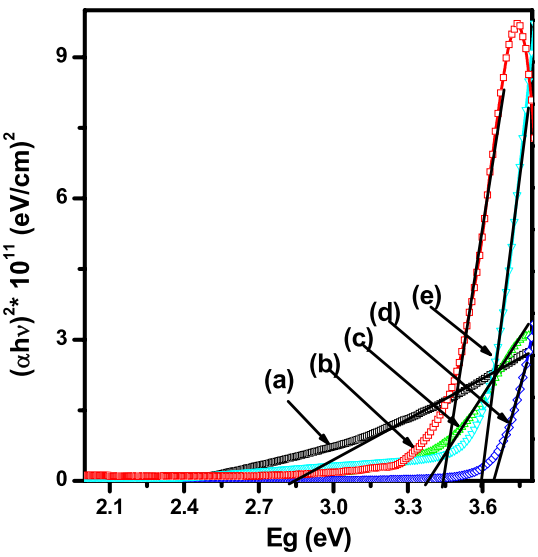

Fig. 5 Plot of $(\alpha h\nu)^2$ versus $(h\nu)$ for annealed ZnS thin films prepared with ***a*** 0 M, ***b*** 0.5 M, ***c*** 1.0 M, ***d*** 1.5 M, ***e*** 2.5 M HyH concentrations

smaller particles. The band gap decreases upon annealing the samples as a counter part of as-deposited layer due to enhancement in the particle size. The film deposited in absence of HyH estimates lower band gap than that of the bulk ZnS probably due to the presence of $Zn(OH)_2$ which is further confirmed by XRD analysis. Thin films prepared with 1.0 M HyH were found to be uniformly grown with compact and granular surface therefore; this sample was

Table 3 A summary of band gap values estimated from UV–Vis absorption spectra for as-deposited and annealed ZnS thin films deposited in presence of various HyH concentrations

ZnS samples (concentration of HyH in M)	Band gap (E_g) (eV)	
	As-deposited	Annealed
0	2.87	2.77
0.5	3.58	3.46
1.0	3.64	3.50
1.5	3.70	3.65
2.5	3.80	3.71

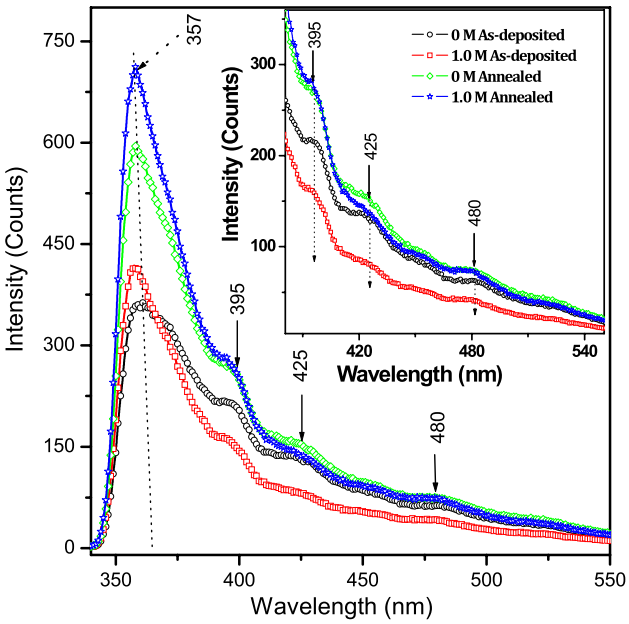

Fig. 6 PL spectra of as-deposited and annealed ZnS films deposited in presence of 1.0 M HyH. The enlarged PL spectra for higher wavelength is given in *inset*

chosen to study the photoluminescence and electrical properties. The room temperature PL spectra recorded at excitation wavelength 325 nm of as-deposited and annealed ZnS thin films obtained with 0 M and 1.0 M HyH is shown in Fig. 6. Four distinct peaks at 357, 395, 425 and 480 nm were observed to all PL spectra's. The narrow UV emission peak attributed at 357 nm corresponds to near-band-edge emission originated from the recombination of free excitons in ZnS. The broadening observed to UV-emission peak for as-prepared layer deposited without HyH could be associated to the growth of non-uniform size particles and the contribution from glass substrate. On the contrary, a sharp UV-emission peak with blue shift was attributed for the samples grown with 1.0 M HyH. The observed blue shift is proposed due to the growth of small size particles. Upon

annealing intensity of this peak was found to be increased. The emission bands centered at 395 and 425 nm could be assigned to stoichiometric vacancies (defect states) or interstitial impurities, possibly at the surface of the ZnS layer. The emission band centered at 395 nm corresponds to the Zn vacancy (V_{Zn}), whereas 425 nm corresponds to the Zn interstitial (Zn_i) and/or S interstitial (S_i) [24–26]. The intensity of these peaks decreases with addition of HyH. A small shoulder noticed at 480 nm may be assigned to the sulfur vacancy (V_s) [27].

3.5 FTIR analysis

Fourier transform infrared (FTIR) spectra measured at room temperature for as-deposited and annealed samples deposited with 0 and 1 M HyH are depicted in Figs. 7 and 8, respectively. A broad absorption peak observed in the range of 3000–3641 cm^{-1} correspond to –OH group, which confirm the existence of water molecules absorbed at the surface or formation of hydroxides. This peak was reduced for the annealed samples. The features attributed around 1146, 1500–1650 and 2343 cm^{-1} are assigned to C=O stretching mode arising from absorption of atmospheric CO_2 on to the surface. The peak exhibited at 578 cm^{-1} is assigned to ZnS band (i.e., corresponding to sulphides) [28, 29]. All peaks observed in FTIR spectra for both as-deposited and annealed samples grown with 0 M HyH and 1.0 M HyH are very similar.

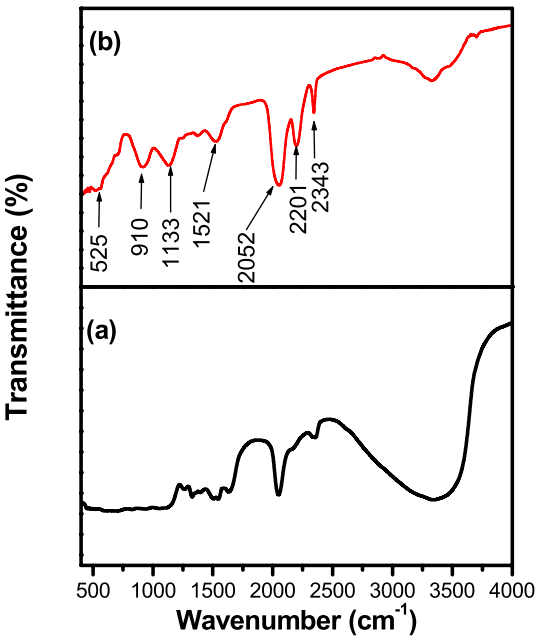

Fig. 7 FTIR spectra of as-deposited (**a**) and annealed (**b**) ZnS films deposited without HyH

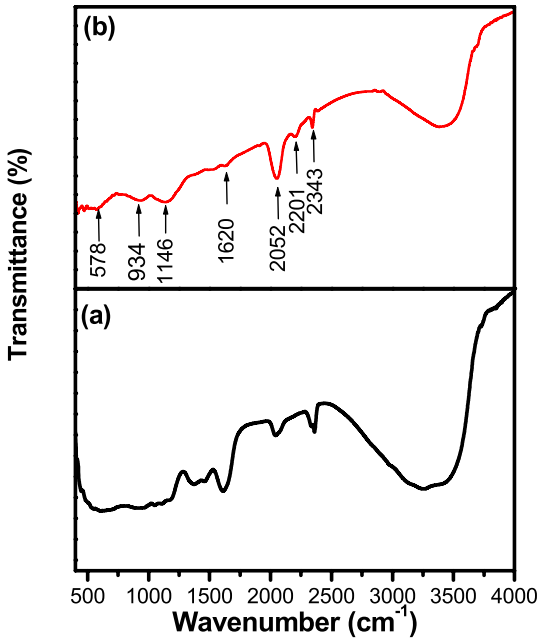

Fig. 8 FTIR spectra of as-deposited (**a**) and annealed (**b**) ZnS films deposited in presence of 1.0 M HyH

3.6 Electrical (I–V and C–V) properties

Figure 9 shows the current density–voltage (J–V) characteristics of the annealed ZnS films deposited with 0 and

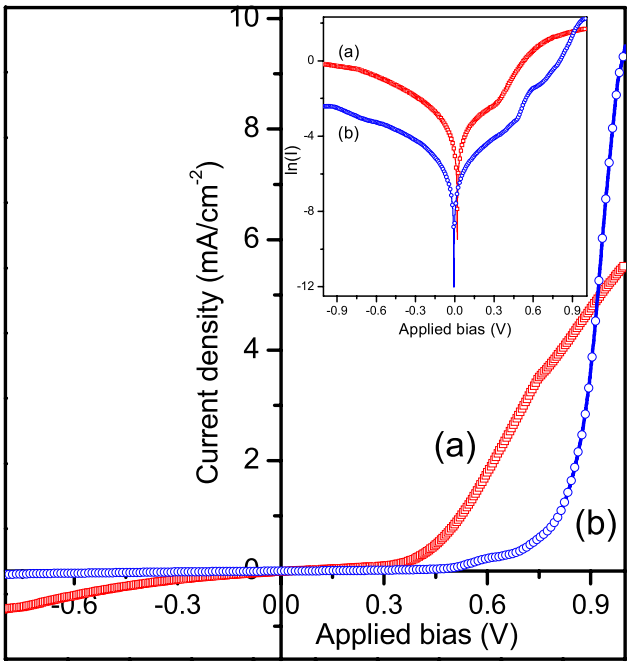

Fig. 9 I–V characteristics of annealed ZnS thin films deposited in presence of 0 M (***a***) and 1.0 M (***b***) HyH. *Inset* depicts the semi-logarithmic curve

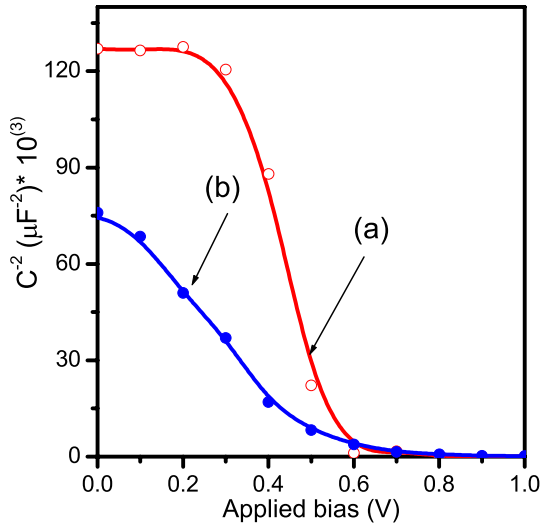

Fig. 10 Mott–schottky characteristics of annealed ZnS thin films deposited at 0 M (***a***) and 1.0 M (***b***) HyH

Table 4 A summary of electrical parameters obtained from capacitance–voltage measurements of ZnS/Al Schottky diodes

Parameter	0 M HyH	1.0 M HyH
Capacitance, $(C)_{V=0}$ (nF)	3.68	2.89
Flat band potential, V_{fb} (eV)	0.49	0.54
Carrier concentration, N_A (cm^{-3})	1.39×10^{17}	4.87×10^{18}

1.0 M HyH concentrations. Al metal contacts of diameter 2 mm were prepared on to FTO/ZnS layers by thermal evaporation technique. Schottky behavior was observed for both layers. It is noteworthy that the diode prepared with 1 M HyH was close to ideal. A high reverse current measured for the sample prepared without HyH could be due to the leaky behavior of diode at high reverse bias. The semi-logarithmic graph of current versus voltage is shown in the inset of Fig. 9. The values of the ideality factor (η) were calculated from the slope of straight line to the lower region of forward bias using the following equation [30]:

$$\eta = \frac{q}{kT}\left(\frac{dV}{d(\ln I)}\right) \tag{6}$$

where q, V, η, k, T and I are the charge of electron, applied voltage, ideality factor, Boltzmann constant temperature and diode current, respectively.

The values of ideality factor, 1.71 and 1.24 were calculated for the annealed ZnS layers prepared with 0 and 1 M HyH, respectively. For an ideal diode, the ideality factor should be close to unity. The value of ideality factor measured greater than unity could be due to the Fermi level pinning at the interface or relatively large voltage drops at the interface region. The reduced value of the ideality factor calculated for the sample prepared with HyH, could be proposed due to the uniform and compact deposition of ZnS over the entire region.

A capacitance–voltage measurement was performed at frequency 10 kHz to determine the doping concentrations and flat band potentials using Eq. (7) [31]. The measurements performed for annealed samples prepared without and 1.0 M HyH are given in Fig. 10.

$$\frac{1}{C^2} = \frac{2}{qN_A A^2 \varepsilon} V \tag{7}$$

where C, V, N_A, q and ε is the space charge capacitance, applied potential, concentration of acceptors, electronic charge and relative permittivity, respectively. The capacitance, flat band potential and carrier concentration evaluated from the gradient of the graph is given in Table 4. High doping concentration ~10^{18} cm^{-3} was calculated for the ZnS layers deposited with 1.0 M HyH as a counter part of 10^{17} cm^{-3} for without HyH, which is proposed due to higher concentration of metallic zinc and well adherent, continuous and uniform grain growth.

4 Conclusions

ZnS thin films have been successfully deposited on FTO and glass substrates using chemical bath deposition method. Nanocrystalline ZnS layers having cubic crystal structure were deposited with HyH.TEM results are in good agreement with XRD analysis. Granular, Uniform and compact layers were deposited over the entire substrate in presence of HyH. Nearly stoichiometric layers were obtained upon annealing the samples prepared in presence of HyH. The energy band gap ~3.80 eV was measured for ZnS layers prepared with HyH revealed the growth of nanocrystalline material. A strong UV emission corresponds to band-edge transition with some defect like vacancies was observed to all samples confirmed by photoluminescence studies. The ideality factor for the ZnS layers prepared with 0 M and 1.0 M HyH were obtained ~1.71 and 1.24, respectively. The capacitance–voltage plots behave according to Schottky–Mott theory. The doping concentrations ~10^{17} and 10^{18} cm^{-3} were calculated for the layers deposited with 0 and 1.0 M HyH, respectively.

Acknowledgements The authors would like to thank the DST (SERI), DST/TM/SERI/FR/124(G), DRDO, (ERIP/ER/10003866/M/01/1388) and BARTI for financial support.

References

1. A. Goudarzi, G.M. Aval, R. Sahraei, H. Ahmadpoor, Thin Solid Films **516**, 4953 (2008)

2. C. Ma, D. Moore, J. Le, Z.L. Wang, Adv. Mater. **15**, 228 (2003)
3. C. Lu, Z. Cui, Z. Li, B. Yang, J. Shen, J. Mater. Chem. **13**, 526 (2003)
4. P. Jackson, D. Hariskos, E. Lotter, S. Paetel, R. Wuerz, R. Menner, W. Wischmann, M. Powalla, Prog. Photovolt. Res. Appl. **19**, 894 (2011)
5. M.A. Green, K. Emery, Y. Hishikawa, W. Warta, E.D. Dunlop, Prog. Photovolt. Res Appl. **21**, 1 (2013)
6. D. Hariskos, S. Spiering, M. Powalla, Thin Solid Films **480–481**, 99 (2005)
7. T. Nakada, M. Hongo, E. Hayashi, Thin Solid Films **431–432**, 242 (2003)
8. G.L. Agawane, S.W. Shin, M.S. Kim, M.P. Suryawanshi, K.V. Gurava, A.V. Moholkar, J.Y. Lee, J.H. Yun, P.S. Patil, J.H. Kim, Curr. Appl. Phys. **13**, 850 (2013)
9. A. Ennaoui, M. Weber, R. Scheer, H. J. Lewerenz, Sol. Energy Mater. Sol. Cells **54**, 277 (1998)
10. W. Eiselea, A. Ennaouia, P. Schubert-Bischoffa, M. Giersiga, C. Pettenkofera, J. Krausera, M. Lux-Steinera, S. Zweigartb, F. Karg, Sol. Energy Mater. Sol. Cells **75**, 17 (2003)
11. F. Engelhardt, L. Bornemann, M. Kontges, Th. Meyer, J. Parisi, E. Pschorr-Schoberer, B. Hahn, W. Gebhardt, W. Riedl, U. Rau, Prog. Photovolt. Res. Appl. **7**, 423 (1999)
12. B. Mari, M. Mollar, D. Soro, R. Henriquez, R. Scherebler, H. Gomez, Int. J. Electrochem. Sci. **8**, 3510 (2013)
13. G. Gordillo, C. Calderlon, Sol. Energy Mater. Sol. Cells **77**, 163 (2003)
14. P. Vasekar, T. Dhakal, L. Ganta, D. Vanhart, S. Desu. Thin Solid Films **524**, 86 (2012)
15. S. Yano, R. Schroeder, B. Ullrich, R.H. Sakai, Thin Solid Films **423**, 273 (2003)
16. R. Zhang, B. Wang, L. Wei, Mater. Chem. Phys. **112**, 557 (2008)
17. E.Y.M. Lee, N.H. Tran, R.N. Lamb, Appl. Surf. Sci. **241**, 493 (2005)
18. Y.S. Kim, S.J. Yun, Appl. Surf. Sci. **229**, 105 (2004)
19. E. Bacaksiz, O. Gorur, M. Tomakin, E. Yanmaz, M. Altunba, Mater. Lett. **61**, 5239 (2007)
20. N.I. Kovtyukhova, E.V. Buzaneva, C.C. Waraksa, T.E. Mallouk, Mater. Sci. Eng. B **69**, 411 (2000)
21. N. Fathy, R. Kobayashi, M. Ichimura, Mater. Sci. Eng. B **107**, 271 (2004)
22. J.M. Dafia, J. Herrero, J. Electrochem. Soc. **141**, 1 (1994)
23. K. Ahn, J.H. Jeon, S.Y. Jeong, J.M. Kim, H.S. Ahn, J.P. Kim, E.D. Jeong, C.R. Cho, Curr. Appl. Phys. **12**, 1465 (2012)
24. H.Y. Lu, S.Y. Chu, S.S. Tan, J. Cryst. Growth **269**, 385 (2004)
25. P. Prathap, N. Revathi, Y.P. Venkata Subbaiah, K.T. Ramakrishna Reddy, R.W. Miles, J. Phys. Cond. Matter **20**, 035205 (2008)
26. K. Nagamani, N. Revathi, P. Prathap, Y. Lingappa, K.T. Ramakrishna Reddy, Curr. Appl. Phys. **12**, 380 (2012)
27. N. Karar, F. Singh, B.R. Mehta, J. Appl. Phys. **95**, 656 (2004)
28. L.T. Chiem, L. Huynh, J. Ralston, D.A. Beattie, J. Colloid. Interface Sci. **297**, 54 (2006)
29. G. Murugadoss, J. Lumin. **131**, 2216 (2011)
30. B.G. Streetmann, S.K. Banerjee, *Solid State Electronic Devices*, 6th edn. (PHI Learning Pvt. Ltd., New Delhi, 2006), p. 229
31. A. Vijayakumar, T. Du, K.B. Sundaram, Appl. Surf. Sci. **242**, 168 (2005)